Bulletin of the JSME Vol.12, No.2, 2017
Journal of Thermal Science and Technology

MHD couple stress nanofluid flow in a permeable wall channel with entropy generation and nonlinear radiative heat

Oluwole Daniel MAKINDE* and Adetayo Samuel EEGUNJOBI**
*Faculty of Military Science, Stellenbosch University, Private Bag X2, Saldanha 7395, South Africa
**Mathematics Department, Namibia University of Science and Technology, Windhoek, Namibia
E-mail: samdet1@yahoo.com

Received: 1 May 2017; Revised: 13 July 2017; Accepted: 22 October 2017

Abstract
In this paper, both first and second laws of thermodynamics are employed to examine the combined effects of nonlinear thermal radiation, buoyancy forces, thermophoresis and Brownian motion on entropy generation rate in hydromagnetic couple stress nanofluid flow through a vertical channel with permeable walls. The model equations of momentum, energy balance and nanoparticle concentration are obtained and tackled numerically using a shooting technique coupled with Runge-Kutta-Fehlberg integration scheme. The numerical results for velocity, temperature and nanoparticles concentration profiles are utilised to determine the skin friction, Nusselt number, Sherwood number, entropy generation rate and Bejan number. It is found that the entropy production in the flow system can be effectively minimized by regulating the values of the thermophysical parameters for efficient operation. Some other interesting results are displayed graphically and discussed quantitatively.

Keywords : MHD channel flow, Couple stress nanofluid, Thermal radiation, Entropy generation, Suction/Injection

1. Introduction

Non-Newtonian fluid flow behaviour with heat and mass transfer is frequently encountered in many engineering and industrial flow processes. An illustrative example of non-Newtonian fluid flow with heat and mass transfer is found in oil reservoir engineering in connection with the production of heavy crude oils. This process involves the injection of steam or heat generation sources for the purpose of increasing the crude oil temperature. The increase in crude oil temperature reduces its viscosity and thus, enhances its mobility resulting in improved oil production flow rates. The simulation of non-Newtonian fluid flow phenomena is therefore of importance to industry. One such non-Newtonian fluid model is the couple stress fluid. The theory of couple stress fluids pioneered by Stokes (1966) allows the rotational field to be defined in terms of the velocity field itself and the rotation vector equals one half the curl of the velocity vector. It is a generalization of the classical theory of viscous fluids with the presence of couple stresses and body couples in the fluid medium. Couple stress fluid model has several industrial and scientific applications which comprise pumping fluids such as synthetic fluids, polymer thickened oils, liquid crystal, animal blood, synovial fluid present in synovial joints and the theory of lubrication as seen in Naduvinamani *et al.* (2003), Lin and Hung (2007) and Adesanya and Makinde (2012). Moreover, it is well known that heating / cooling in an industrial process create a number of advantages like energy saving, reduction in processing time and also the superiority of the manufactured goods. Since the thermal behaviour of working fluids determines the heat transfer efficiency, a major task for industrial necessity is to enhance the thermal conductivity of the working fluid. This is achieved by suspending nano-sized particles into the base fluid as pioneered by Choi (1995). This mixture is used to enhance the rate of heat transfer through its higher thermal conductivity compared to the base fluid. The enhance heat transfer rate of nanofluid is due to higher thermal conductivity of the embedded metallic or non-metallic nanoparticles as compared to the base fluid. Nanofluids have many practical applications such as in chillers, refrigerator-freezers, nuclear reactors, in space vehicles, in cooling of engine electronic equipment,

Paper No.17-00252
[DOI: 10.1299/jtst.2017jtst0033]

transformer oil and heat exchanging devices, etc., In view of this several researchers Wang et al (1999), Eastman et al (2001), Buongiorno (2006), Makinde et al (2016a), Makinde et al (2016b), Makinde et al (2016c) conducted theoretical or experimental investigation on flow and heat transfer behavior nanofluid comprehensively. Selvakumar and Dhinakaran (2017) investigated numerically the convective forced heat transfer around a circular cylinder using nanofluids by employing a mixture model based multi-phase modelling (MPM) approach. Their results revealed higher heat transfer rates in MPM with slip velocity. Meanwhile, thermal radiation plays a very important role in the design of many advanced energy conversion systems that are operating at high temperature or using nanofluids, Rosseland (1936), Ozisik (1973). The effects of radiation also become more important when the difference between the surface and the ambient temperature is large. Free convection flow in a porous medium with thermal radiation was numerically investigated by Reptis (2009). Abbas *et al*. (2016) presented a similarity solution for the combined effects of magnetic field and thermal radiation on boundary layer flow of nanofluid over a stretching sheet with velocity slip.

Entropy production and its minimization have been considered as an effective instrument for improving the performance of any flow with heat and mass transfer processes. The quality of energy in a system decreases with the production of entropy. In order to enhance the quality of energy, it is important to determine the sources of entropy generation and examine the flow parameters which minimize the production of entropy. Bejan (1996) pioneered the theoretical study of entropy generation minimization in a flow with heat transfer process based on the thermodynamics second law. Thereafter, several works on entropy generation minimisation have appeared in the literature Woods (1975), Mkwizu and Makinde (2015), Das et al. (2015), Makinde and Eegunjobi (2016), Eegunjobi and Makinde (2017a) and Eegunjobi and Makinde (2017b). Entropy generation rate produced by natural circulation in a square cavity filled with Al_2O_3 nanofluid was numerically studied by Cho (2014). Leong *et al*. (2012) examined the entropy generation rate in three different types of heat exchangers operated with nanofluids. Mahmoudi *et al*. (2013) investigated the effects of magnetic field on entropy generation rate in a trapezoidal enclosure with Copper–water nanofluid. Their result revealed that both dispersed nanoparticles and magnetic field enhance the heat transfer irreversibility. To the best of authors' knowledge, the combined effects of buoyancy forces, suction/injection, magnetic field, viscous and Joule heating on entropy production in a conducting non-Newtonian couple stress nanofluid has not been reported in the literature yet. Meanwhile, the hydromagnetic mixed convective flow of couple stress nanofluid with heat transfer over a permeable surface in the presence of radiative heat absorption appears to be increasingly important due to its wide applications in the field of micro-electro-mechanical-systems (MEMS), such as micro MHD pumps, micro-electronic devices, rapid mixing of fluids in biological processes, biological transportation, drug delivery and heat exchanger, Dulal *et al.* (1988), Chiang *et al.* (2004), Leong *et al.* (2012). Surface permeability plays a very vital role in micro-mixing of biological fluid, it enhances transpiration process to take place at the boundaries in a micro system, whereby suction is exerted in order to remove reactants while injection is applied to add reactants in the process. Therefore, the present article deals with the first and second law analyses of mixed convection of an electrically conducting couple stress nanofluid in a vertical channel with permeable walls in the presence of a magnetic field. We employed shooting method with Runge-Kutta-Fehlberg integration technique to study the problem. The discussion regarding the influence of governing parameters on different flow fields and entropy production are given numerically through graphs.

2. Mathematical Formulation

We consider fully developed the hydromagnetic steady flow of an incompressible, electrically and thermally conducting and radiating couple stress nanofluid between two infinite vertical permeable parallel walls at $y = 0$ and $y = a$ in the presence of a uniform transverse magnetic field of strength B_0 which is applied parallel to y -axis. The magnetic Reynolds number and the induced electric field are assumed to be small and negligible. The flow within the channel is induced due to the combined action of applied uniform pressure gradient along x -direction and the suction/injection velocity (V) at the channel walls. The channel left wall is convectively heated with hot fluid at temperature T_f with heat transfer coefficient h_f while the right wall is maintained at temperature T_1. Heat transfer analysis is carried out in the presence of thermophoresis due to the presence of nanoparticles, Brownian motion, viscous dissipation thermal radiation and Ohmic heating. The physical model of the problem is presented in figure 1.

[DOI: 10.1299/jtst.2017jtst0033]

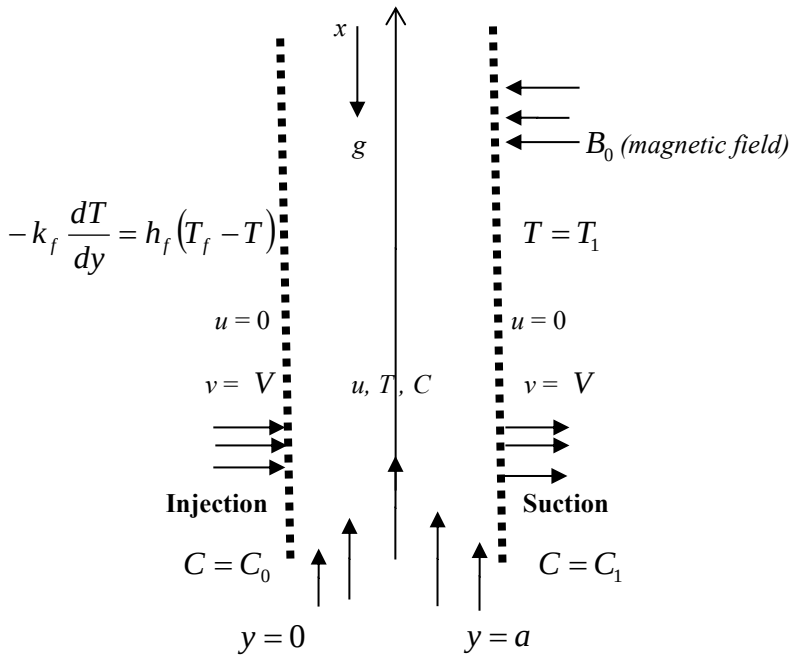

Figure 1. Physical model of the problem.

Following the Buongiorno (2006) and considering the above assumptions, the governing equations for steady flow of a viscous, incompressible, electrically and thermally conducting nanofluid together with the volumetric entropy generation rate can be written as Stokes (1966), Naduvinamani et al. (2003), Lin and Hung (2007), Adesanya and Makinde (2012), Makinde et al. (2016a), Makinde and Eegunjobi (2017a, b):

$$-V\frac{du}{dy} = -\frac{1}{\rho_f}\frac{\partial P}{\partial x} + \upsilon_f \frac{d^2u}{dy^2} - \frac{\delta}{\rho_f}\frac{d^4u}{dy^4} - \frac{\sigma B_0^2 u}{\rho_f} + g\beta_1(T - T_f) + g\beta_2(C - C_1) \tag{1}$$

$$-V\frac{dT}{dy} = \frac{k_f}{\rho_f c_{pf}}\frac{d^2T}{dy^2} + \frac{\upsilon_f}{c_{pf}}\left(\frac{du}{dy}\right)^2 + \frac{\delta}{\rho_f c_{pf}}\left(\frac{d^2u}{dy^2}\right)^2 - \frac{1}{\rho_f c_{pf}}\frac{\partial q_r}{\partial y} + \frac{\sigma B_0^2 u^2}{\rho_f c_{pf}} + \tau\left[D_B\frac{dT}{dy}\frac{dC}{dy} + \frac{D_T}{T_f}\left(\frac{dT}{dy}\right)^2\right], \tag{2}$$

$$-V\frac{dC}{dy} = D_B\frac{d^2C}{dy^2} + \frac{D_T}{T_f}\frac{d^2T}{dy^2}, \tag{3}$$

$$E_G = \frac{k_f}{T_f^2}\left(1 + \frac{16\sigma^* T^3}{3k^* k_f}\right)\left(\frac{dT}{dy}\right)^2 + \frac{\mu_f}{T_f}\left(\frac{du}{dy}\right)^2 + \frac{\delta}{T_f}\left(\frac{d^2u}{dy^2}\right)^2 + \frac{\sigma B_0^2 u^2}{T_f} + \frac{D_B}{C_0}\left(\frac{dC}{dy}\right)^2 + \frac{D_B}{T_f}\frac{dC}{dy}\frac{dT}{dy}. \tag{4}$$

The appropriate boundary conditions for the fluid velocity, temperature and the nanoparticles volume fraction are given as

$$u = \frac{d^2u}{dy^2} = 0, \quad -k_f\frac{dT}{dy} = h_f(T_f - T), \; C = C_0, \text{ at} \quad y = 0, \tag{5}$$

[DOI: 10.1299/jtst.2017jtst0033]

$$u = \frac{d^2u}{dy^2} = 0, \quad T = T_1, \quad C = C_1, \text{at} \quad y = a, \tag{6}$$

where u is the axial velocity, h_f is wall heat transfer coefficient, μ_f is the dynamic viscosity, ρ_f is the nanofluid density, E_G is the entropy generation rate, T is the fluid temperature, c_{pf} is specific heat at constant pressure, σ is the electrical conductivity, g is the gravitational acceleration, δ is the fluid particle size effect due to couple stresses, V is the wall suction/injection velocity, C_0 is the nanoparticles concentration at the left wall, C_1 is the nanoparticles concentration at the right wall, T_1 is the channel right wall temperature, β_1 is the thermal expansion coefficient, β_2 is the concentration expansion coefficient, k_f is the thermal conductivity of the nanofluid, D_B and D_T are the Brownian diffusion coefficient and the thermophoretic diffusion coefficient. By assuming Rosseland approximation Rosseland (1936), Ozisik (1973) Raptis (2009), the radiative heat flux is taken as

$$q_r = -\frac{4\sigma^*}{3k^*}\frac{\partial T^4}{\partial y} = -\frac{16\sigma^* T^3}{3k^*}\frac{\partial T}{\partial y}, \tag{7}$$

Where σ* is the Stefan-Boltzman constant and k^* is the mean absorption coefficient. We introduce the dimensionless variables and parameters as follows:

$$\eta = \frac{y}{a}, X = \frac{x}{a}, \theta = \frac{T - T_f}{T_1 - T_f}, \upsilon_f = \frac{\mu_f}{\rho_f}, w = \frac{ua}{\upsilon_f}, \Pr = \frac{\rho_f \upsilon_f c_{pf}}{k_f}, \gamma = \frac{T_f}{T_1 - T_f}, Le = \frac{\alpha_f}{D_B},$$
$$n_1 = \frac{D_B \gamma (C_0 - C_1)}{k_f}, Ec = \frac{\upsilon_f^2}{c_{pf}(T_1 - T_f)a^2}, \lambda = \frac{\delta}{\rho_f \upsilon_f a^2}, A = -\frac{\partial \bar{P}}{\partial X}, M = \frac{\sigma B_0^2 a^2}{\rho_f \upsilon_f},$$
$$Nt = \frac{\tau D_T (T_1 - T_f)}{T_f \alpha_f}, n_2 = \frac{\gamma (C_0 - C_1)}{C_0}, Nr = \frac{16\sigma^* (T_1 - T_f)^3}{3k^* k_f}, Ns = \frac{E_G a^2 T_f^2}{k_f (T_1 - T_f)^2}, \tag{8}$$
$$Gr_c = \frac{g\beta_2 (C_0 - C_1)a^3}{\upsilon_f^2}, Nb = \frac{\tau D_B (C_0 - C_1)}{\alpha_f}, \text{Re} = \frac{Va}{\upsilon_f}, \bar{P} = \frac{a^2 p}{\rho_f \upsilon_f^2}, \tau = \frac{\rho_s c_{ps}}{\rho_f c_{pf}},$$
$$Gr_T = \frac{g\beta_1 (T_1 - T_f)a^3}{\upsilon_f^2}, Bi = \frac{ah_f}{k_f}, \varphi = \frac{C - C_1}{C_0 - C_1}, \alpha_f = \frac{k_f}{\rho_f c_{pf}}.$$

Substituting equation (8) into equations (1)-(7), we obtain,

$$\frac{d^2 w}{d\eta^2} - \lambda \frac{d^4 w}{d\eta^4} + \text{Re}\frac{dw}{d\eta} - Mw + Gr_T \theta + Gr_c \varphi + A = 0, \tag{9}$$

$$\left[1 + Nr(\theta + \gamma)^3\right]\frac{d^2\theta}{d\eta^2} + 3Nr(\theta + \gamma)^2\left(\frac{d\theta}{d\eta}\right)^2 + \Pr \text{Re}\frac{d\theta}{d\eta}$$
$$+ \Pr Ec\left[\left(\frac{dw}{d\eta}\right)^2 + \lambda\left(\frac{d^2 w}{d\eta^2}\right)^2 + Mw^2\right] + Nb\frac{d\theta}{d\eta}\frac{d\varphi}{d\eta} + Nt\left(\frac{d\theta}{d\eta}\right)^2 = 0, \tag{10}$$

$$\frac{d^2\varphi}{d\eta^2} + \Pr \text{Re}\, Le\frac{d\varphi}{d\eta} + \frac{Nt}{Nb}\frac{d^2\theta}{d\eta^2} = 0, \tag{11}$$

$$Ns = \left[1 + Nr(\theta + \gamma)^3\right]\left(\frac{d\theta}{d\eta}\right)^2 + \Pr Ec\gamma\left[\left(\frac{dw}{d\eta}\right)^2 + \lambda\left(\frac{d^2 w}{d\eta^2}\right)^2 + Mw^2\right] + n_1\left[\frac{d\theta}{d\eta}\frac{d\varphi}{d\eta} + n_2\left(\frac{d\varphi}{d\eta}\right)^2\right], \tag{12}$$

with

[DOI: 10.1299/jtst.2017jtst0033]

$$w = \frac{d^2 w}{d\eta^2} = 0,\ \frac{d\theta}{d\eta} = Bi\theta, \varphi = 1 \qquad \text{at} \qquad \eta = 0, \tag{13}$$

$$w = \frac{d^2 w}{d\eta^2} = 0,\ \theta = 1,\ \varphi = 0 \qquad \text{at} \qquad \eta = 1, \tag{14}$$

Where Pr is the Prandtl number, Re is the suction / injection Reynolds number, Gr_T is the thermal Grashof number, Gr_c is the concentration Grashof number, Bi is the Biot number, λ is the couple stress parameter, Ec is the Eckert number, A is pressure gradient, Nt is the thermophoresis parameter, Nb is the Brownian motion parameter, M is the magnetic field parameter, γ is the temperature difference parameter, Nr is the radiation parameter, n_1 and n_2 are the nanoparticles entropy generation parameters. Other quantities of interest are the skin friction coefficients (Cf), Nusselt number (***Nu***), Sherwood number (***Sh***) and the Bejan number (***Be***) which are given as

$$Cf = \frac{\rho a^2 \tau_w}{\mu^2} = \left.\frac{dw}{d\eta}\right|_{\eta=0,1}, \qquad Nu = -\frac{aq_w}{k_f(T_1 - T_f)} = -\left[1 + Nr(\theta+\gamma)^3\right]\left.\frac{d\theta}{d\eta}\right|_{\eta=0,1},$$

$$Sh = -\frac{aq_m}{D_B(C_0 - C_1)} = -\left.\frac{d\varphi}{d\eta}\right|_{\eta=0,1}, \quad Be = \frac{N_1}{Ns} = \frac{1}{1+B}, \tag{15}$$

where

$$\tau_w = \mu_f \frac{\partial u}{\partial y} - \delta \frac{\partial^3 u}{\partial y^3},\ q_w = -k_f\left(1 + \frac{16\sigma^* T^3}{3k_f k^*}\right)\frac{\partial T}{\partial y}, \quad q_m = -D_B \frac{\partial C}{\partial y}, \tag{16}$$

and

$$N_1 = \left[1 + Nr(\theta+\gamma)^3\right]\left(\frac{d\theta}{d\eta}\right)^2, B = \frac{N_2 + N_3}{N_1}, N_3 = n_1\left[\frac{d\theta}{d\eta}\frac{d\varphi}{d\eta} + n_2\left(\frac{d\varphi}{d\eta}\right)^2\right],$$

$$N_2 = \Pr Ec\lambda\left[\left(\frac{dw}{d\eta}\right)^2 + \lambda\left(\frac{d^2 w}{d\eta^2}\right)^2 + Mw^2\right]. \tag{17}$$

The symbol N_1 represents thermodynamic irreversibility due to thermal radiation absorption and heat transfer, N_2 corresponds to the entropy generation due to combined effects of fluid friction and magnetic field while N_3 is the irreversibility due to nanoparticles concentration. When $0.5 < \boldsymbol{Be} \le 1$, the effects of thermodynamics irreversibility due to thermal radiation absorption and heat transfer dominate the flow system while $0 \le \boldsymbol{Be} < 0.5$ corresponds to the dominant effects of fluid friction, magnetic field and nanoparticles concentration irreversibilities. When $\boldsymbol{Be} = 0.5$, N_1 and combined N_2 and N_3 contribute equally to the entropy generation and Be is the irreversibility ratio. Moreover, the dimensionless model equations (9)-(14) are solved numerically using a shooting method together with Runge-Kutta-Fehlberg integration scheme.

3. Numerical Procedure

The dimensionless equations (9)-(12) coupled with the boundary conditions (13)-(14) are boundary value problem (BVP). We transformed these equations into a set of nonlinear first order ordinary differential equations with some unknown initial conditions to be calculated by shooting technique Na (1979).

Let,

$$w = y_1,\ w' = y_2, w'' = y_3,\ w''' = y_4, \theta = y_5, \theta' = y_6, \varphi = y_7, \varphi' = y_8. \tag{18}$$

[DOI: 10.1299/jtst.2017jtst0033]

The governing equations then become

$$\left.\begin{aligned} y_1' = y_2, y_2' = y_3, y_3' = y_4, y_4' = \frac{1}{\lambda}\left[y_3 + \mathrm{Re}\, y_2 - My_1 + Gr_T y_5 + Gr_c y_7 + A\right] \\ y_5' = y_6, y_6' = -\frac{1}{\left(1+Nr(1+y_5)^3\right)}\left(3Nr(y_5+\gamma)^2 y_6^2 + \mathrm{Pr}\,\mathrm{Re}\, y_6 + \mathrm{Pr}\, Ec\left[y_2^2 + \lambda y_3^2 + My_1^2\right] + Nby_6 y_8 + Nty_6^2\right) \\ y_7' = y_8, y_8' = -\left(\mathrm{Pr}\,\mathrm{Re}\, Ley_7 + \frac{Nt}{Nb} y_6'\right) \end{aligned}\right\}, \quad (19)$$

with the corresponding initial conditions as

$$y_1(0) = 0, y_2(0) = a_1, y_3(0) = 0, y_4(0) = a_2, y_5(0) = a_3, y_6(0) = Bia_3, y_7(0) = 1, y_8(0) = a_4. \quad (20)$$

The values for a_1, a_2, a_3, a_4 in the equation (20) are first guessed and then determined accurately with shooting method via Newton-Raphson's technique for each set of parameter values in equation (19). Fourth-fifth order Runge-Kutta-Fehlberg integration scheme Na (1979) is then employed to tackle the resulting initial value problem numerically with step size Δη=0.01. Thereafter, we obtain the skin friction (Cf), the Nusselt number (Nu), the Sherwood number, the entropy generation rate and the Bejan number as given by equations (15) - (17).

4. Results and Discussion

In order to have better understanding of the behaviour of the couple stress nonafluid velocity, temperature, concentration, skin friction, Nusselt number, Sherwood number, entropy generation rate and the Bejan number, we carried out numerical computation for different parameters that describe the flow. We assumed Pr = 6.2 throughout the numerical computation. In order to validate the accuracy our numerical results, the exact solution for the fluid velocity profiles given by equation (9) is obtained when $A = 1$, $Gr_T = Gr_c = \lambda = 0$ (see equation (21)) and compared with our numerical solution of section 3 in the table below:

$$w(\eta) = \frac{A}{M} - \frac{A\left(e^{-\frac{1}{2}\mathrm{Re} - \frac{1}{2}\sqrt{\mathrm{Re}^2+4M}} - 1\right)e^{\left(-\frac{1}{2}\mathrm{Re} + \frac{1}{2}\sqrt{\mathrm{Re}^2+4M}\right)\eta}}{M\left(e^{-\frac{1}{2}\mathrm{Re} - \frac{1}{2}\sqrt{\mathrm{Re}^2+4M}} - e^{-\frac{1}{2}\mathrm{Re} + \frac{1}{2}\sqrt{\mathrm{Re}^2+4M}}\right)} + \frac{A\left(-1 + e^{-\frac{1}{2}\mathrm{Re} + \frac{1}{2}\sqrt{\mathrm{Re}^2+4M}}\right)e^{\left(-\frac{1}{2}\mathrm{Re} - \frac{1}{2}\sqrt{\mathrm{Re}^2+4M}\right)\eta}}{M\left(e^{-\frac{1}{2}\mathrm{Re} - \frac{1}{2}\sqrt{\mathrm{Re}^2+4M}} - e^{-\frac{1}{2}\mathrm{Re} + \frac{1}{2}\sqrt{\mathrm{Re}^2+4M}}\right)} \quad (21)$$

Table 1: Computations showing comparison between exact and numerical solution (A = 1, $Gr_T = Gr_c = \lambda = 0$).

η	M	Re	Exact Solution $w(\eta)$	Numerical Solution $w(\eta)$
0	0.1	0.1	0.000000000	0.000000000
0.1	0.1	0.1	0.045184454	0.045184454
0.3	0.4	0.3	0.102763739	0.102763739
0.5	0.5	0.5	0.118224785	0.118224785
0.7	1.5	1.0	0.0842894129	0.0842894129
0.9	2.5	2.0	0.0277465628	0.0277465628
1.0	2.0	1.0	0.0000000000	0.0000000000

From the table 1 above, it is noteworthy that both the exact solution in equation (21) and numerical solution obtained using shooting technique coupled with Runge-Kutta-Fehlberg integration scheme perfectly agreed. This serves as a

[DOI: 10.1299/jtst.2017jtst0033]

benchmark and confirmation of the accuracy of our numerical procedures and results obtained in this present study.

4.1 Velocity Profiles

Figures 2-6 show the effects of various parameters variation on the couple stress nanofluid velocity profiles. It is interesting to note that the maximum velocity is observed within the channel core region while the minimum is at the permeable walls. Figure 2 shows the effects of injection/suction Reynolds number and pressure gradient on the velocity profile. It is found that velocity profile decelerates with increasing Reynolds number. Meanwhile in the same figure, a rise in pressure gradient enhances the velocity profile. Figure 3 depicts the effects of the thermal Grashof and concentration Grashof numbers on the nanofluid velocity profile. It is noticed that the rise in each of these parameters enhance the velocity profile. The effects of magnetic field parameter (M) and couple stress parameter (λ) are illustrated in figure 4. It is evident in this figure that both M and λ slowdown the velocity profile. This is due to the fact that as the magnetic field intensity increases, the resisting Lorenz force will increase, consequently, the velocity profile decreases. It is interesting to note that the shear stress rate of couple stress nanofluid decreases with increasing λ, consequently, the flow rate reduces, however, the behaviour becomes Newtonian as the parameter λ tends to zero. Figure 5 presents the influence of the Brownian motion parameter (Nb) and thermophoresis parameter on the nanofluid velocity profile. As the Nb gets larger, the velocity profile rises. This may be attributed to the fact that the nanoparticles within the fluid are empowering to move randomly. Meanwhile, as the Nt increases, the velocity profile declined. The effects of Lewis number (Le) and Biot number (Bi) on nanofluid velocity is displayed in figure 6. It is found that the velocity profile slowdown as Le and Bi increase. This decrease in the velocity profile may the attributed to the convective cooling with heat loss at the left permeable wall as well as increase in the nanofluid thermal diffusivity.

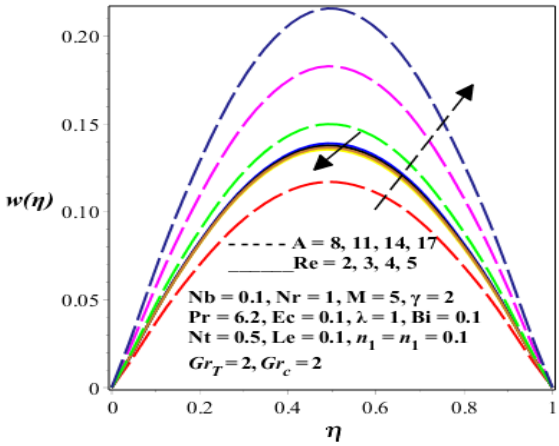

Fig.2: Velocity profile as Re and A increase

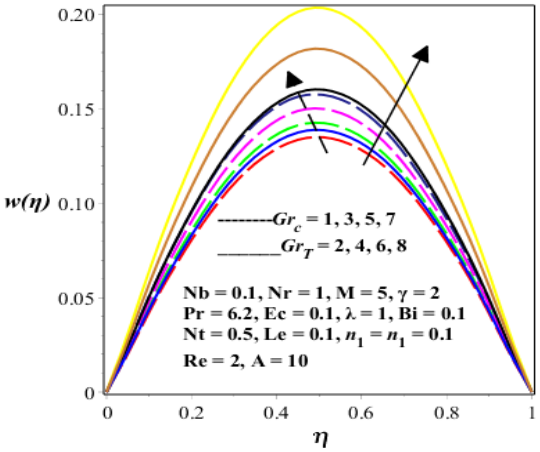

Fig.3: Velocity profile as Gr_T and Gr_c increase

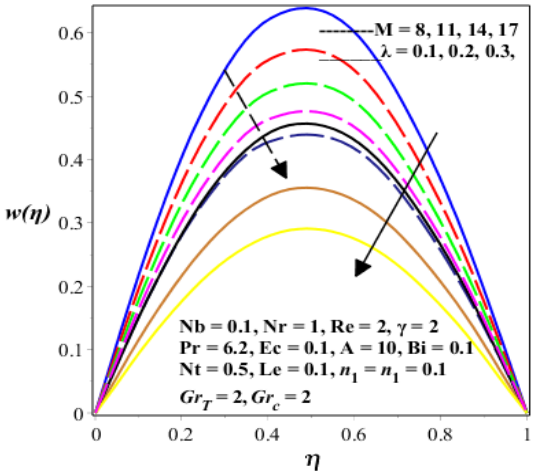

Fig.4: Velocity profile as M and λ increase

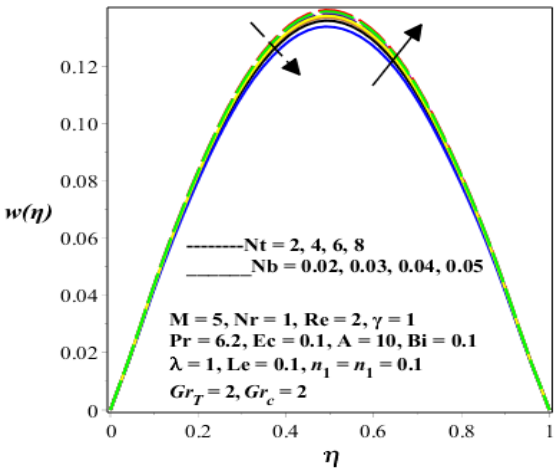

Fig.5: Velocity profile as Nt and Nb increase

[DOI: 10.1299/jtst.2017jtst0033]

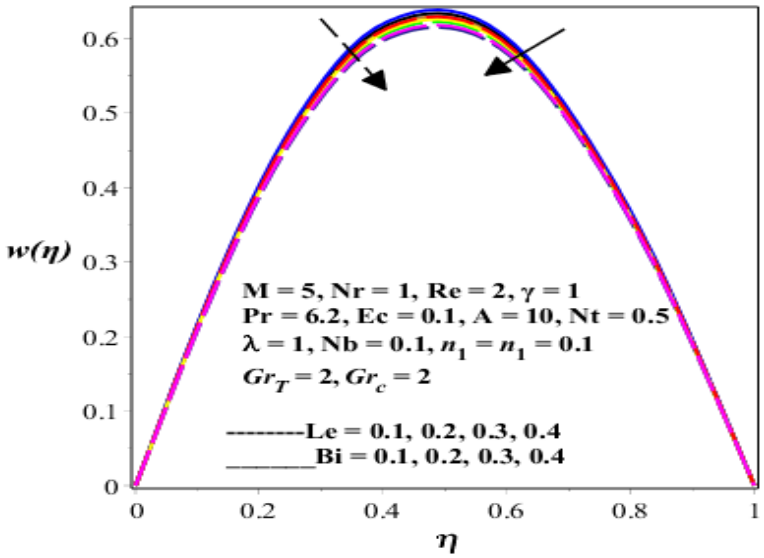

Fig.6: Velocity profile as Le and Bi increase

4.2. Temperature Profiles

Figures 7-11 show the effects of thermophysical parameters on the temperature profile. The effects of Re and A on temperature profile can be seen in figure 7. It is found that an increase in Re and A enhance the nanofluid temperature profile. This is expected, since a rise in pressure gradient enhances internal heat generation due to viscous dissipation and couple stress effects. The influences of the thermal Grashof and concentration Grashof numbers are presented in figure 8. It is found that the temperature profile rises with an increase in both thermal Grashof and concentration Grashof numbers rise. This rise in temperature may be attributed to a combined increase in the both temperature and nanoparticles concentration buoyancy forces. In figures 9-11 we observed that an increase in magnetic field parameter (M), couple stress parameter (λ), Lewis number (Le), Biot number (Bi), and radiation parameter (Nr) and temperature difference parameter substantially decreased the nanofluid temperature profile. Increase in Biot number represents a rise in convective cooling at the left permeable wall with increasing heat loss to the ambient environment, consequently, the radiative heat transfer and temperature difference increase, leading to a drop in nanofluid temperature.

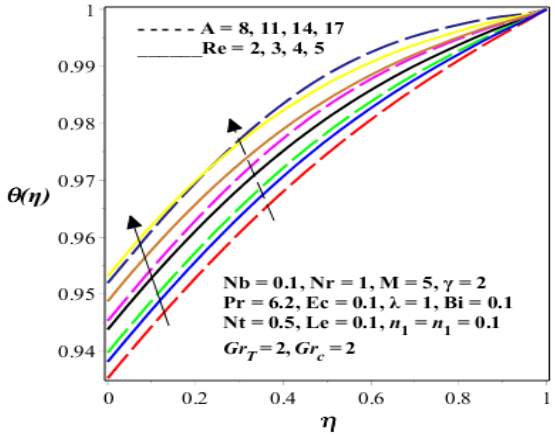

Fig.7: Temperature profile as Re and A increase

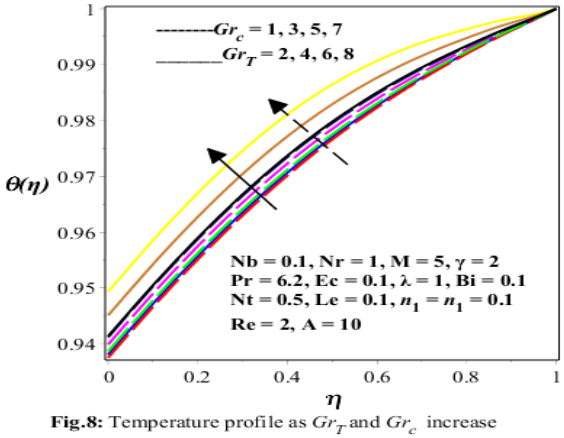

Fig.8: Temperature profile as Gr_T and Gr_c increase

[DOI: 10.1299/jtst.2017jtst0033]

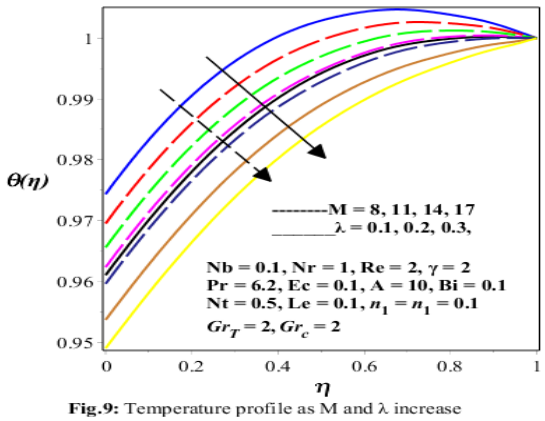

Fig.9: Temperature profile as M and λ increase

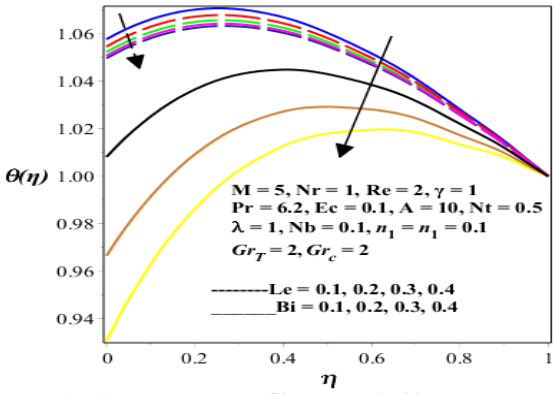

Fig.10: Temperature profile as Le and Bi increase

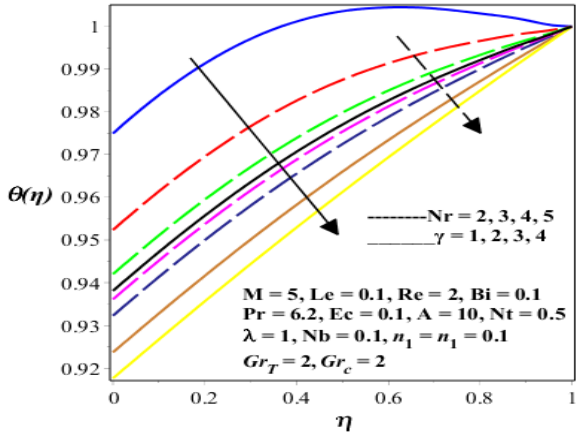

Fig.11: Temperature profile as Nr and γ increase

4.3. Concentration profile

Figures 12-15 illustrate the influence of parameter variations on the nanofluid concentration profile. Generally, the nanoparticles concentration is highest at the left wall and gradually decreases to the prescribe value at the right wall. As pressure gradient and Reynolds number rises, the nanoparticles concentration towards the left wall decreases as depicted in figure 12. This is expected since the combined increase in pressure gradient and Reynolds number increases the suction rate at the left wall and injection at the right wall, consequently, the nanoparticles tend to flow towards the right wall, leading to a decrease in the concentration near the left wall. Figure 13 shows that increase in Brownian motion parameter enhances the nanoparticles concentration flow towards the right wall while a rise in thermophoresis parameter increases the movement of nanoparticles towards the left wall. The influence of Le and Bi on nanofluid concentration profile are depicted in figure 14. This figure shows that nanoparticles concentration moves toward the left wall as Le and Bi are increasing. This means that, a rise Biot number and Lewis number due to convective heat transfer to the ambient will enhance the movement of nanoparticles towards the left wall. Figure 15 shows that nanoparticles concentration increases towards the right wall with a rise in thermal radiation parameter (Nr*)* and temperature difference parameter (γ).

[DOI: 10.1299/jtst.2017jtst0033]

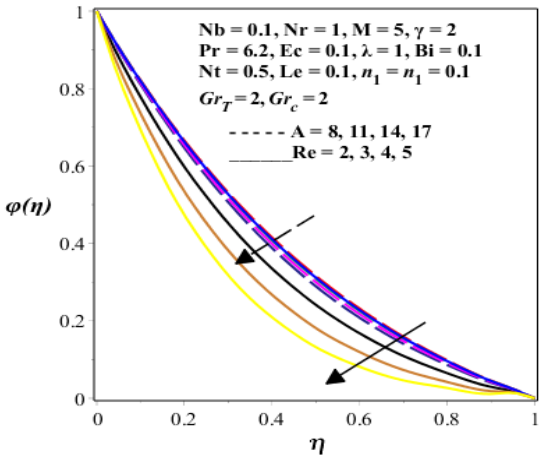

Fig.12: Concentration profile as Re and A increase

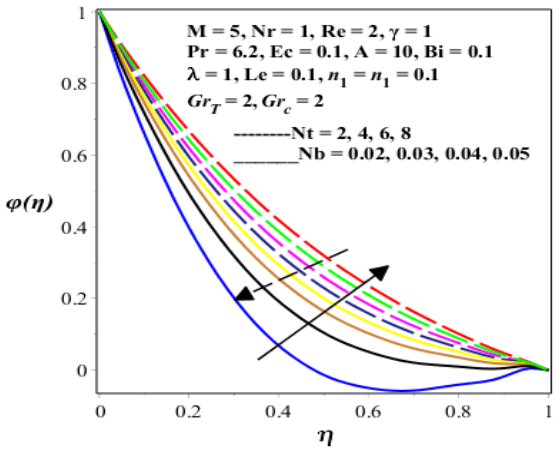

Fig.13: Concentration profile as Nt and Nb increase

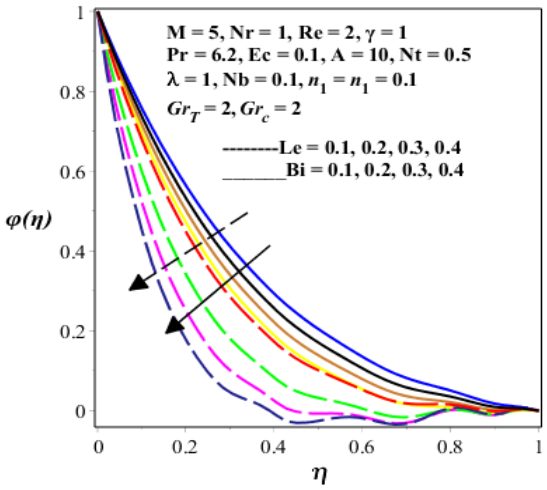

Fig.14: Concentration profile as Le and Bi increase

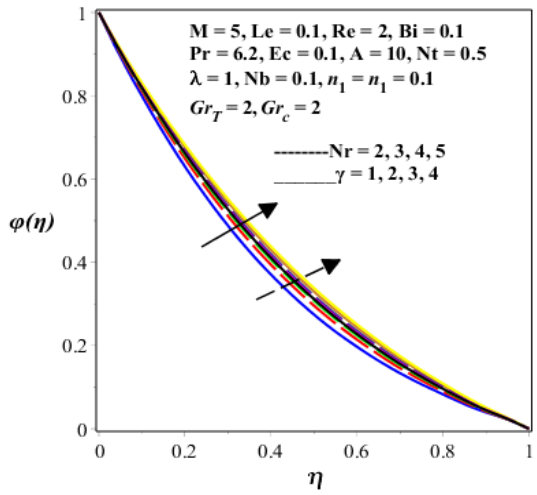

Fig.15: Concentration profile as Nr and γ increase

4.4. Skin Friction, Nusselt number and Sherwood number

The effects of thermophysical parameters on skin friction, Nusselt number and Sherwood number are reflected in figures 16-25. Generally, the skin friction is higher at the right wall due to injection and lower at the left wall due to suction. It is observed in figures 16-19 that skin friction at both walls decrease with an increase in Le, Bi, M and λ. Increase in these parameters cause a decrease in the momentum transfer and shear stress leading to a decrease in the skin friction. Meanwhile, a rise in parameter values of A, Gr_T and Gr_c increase the skin friction at both walls. This can be attributed to an increase in the velocity gradient at both walls as these parameters increase. Figures 20 -21 demonstrate the effects of Bi, Nr, γ and Le on the Nusselt number. It is interesting to note that heat flux at the left wall is enhanced while the heat flux at the right wall decreases with increasing values of Biot number, thermal radiation and temperature different parameter. This may the attributed to convective cooling and heat loss to the ambient at the left wall. Similar effect is observed with increasing Lewis number due to increasing nanofluid thermal diffusivity. Figures 22-25 revealed that the nanoparticle mass transfer rate is enhanced at the left wall and decrease at the right wall with increasing values of Bi, Le, A and Re. This may be attributed to a rise in the nanoparticles concentration gradient at the left wall and a fall in the concentration gradient as these parameter increases. Meanwhile, it is noteworthy that the mass transfer at left wall slowdown with a rise couple stress parameter λ.

[DOI: 10.1299/jtst.2017jtst0033]

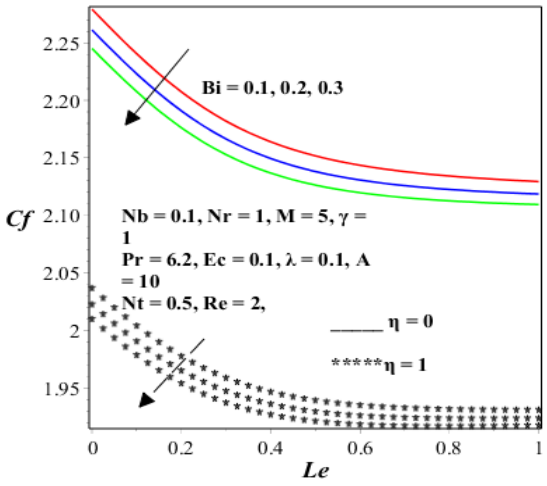

Fig.16: Skin friction as Le and Bi increase

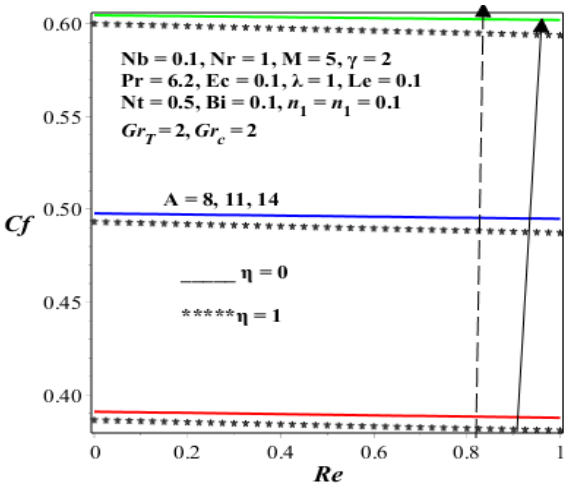

Fig.17: Skin friction as A versus Re increase

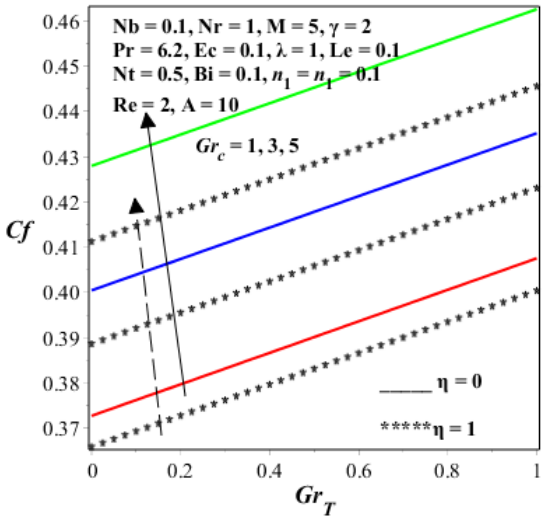

Fig.18: Skin friction as Gr_c versus Gr_T increase

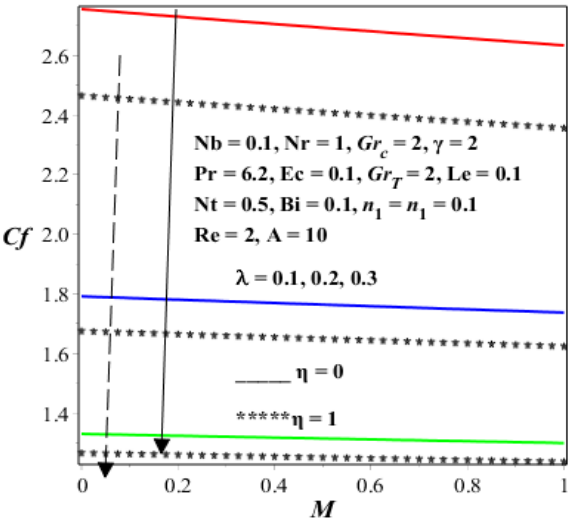

Fig.19: Skin friction as λ versus M increase

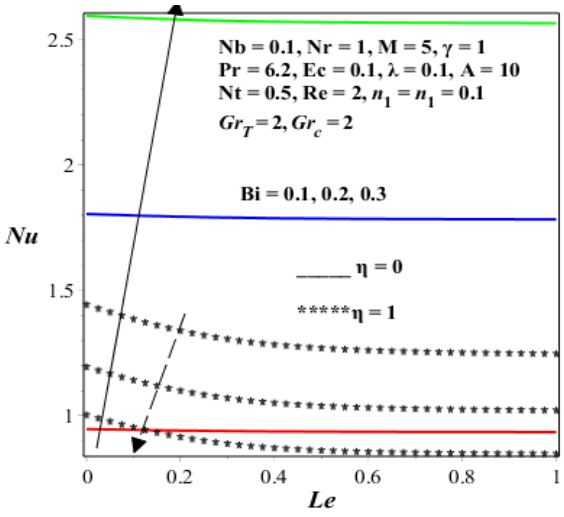

Fig.20: Nusselt number as Bi versus Le increase

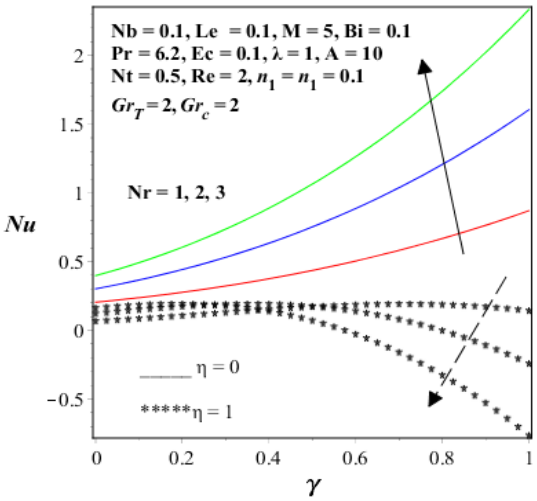

Fig.21: Nusselt number as Nr versus γ increase

[DOI: 10.1299/jtst.2017jtst0033]

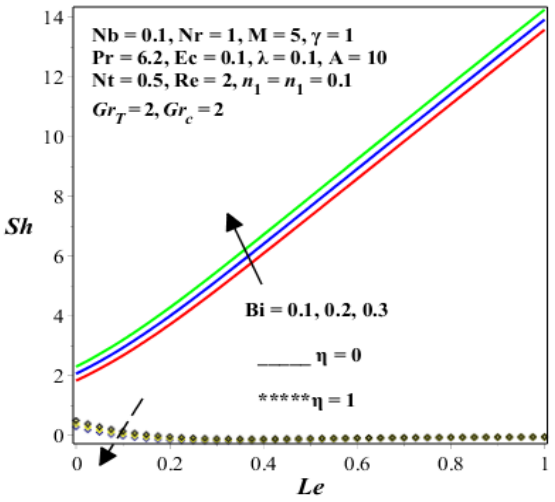

Fig.22: Sherwood number as Le and Bi increase

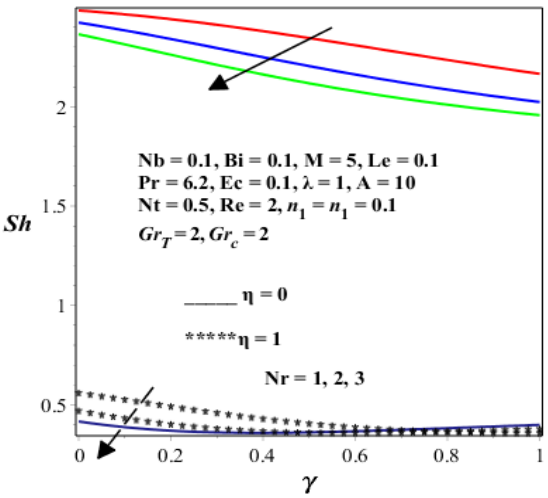

Fig.23: Sherwood number as Nr versus γ increase

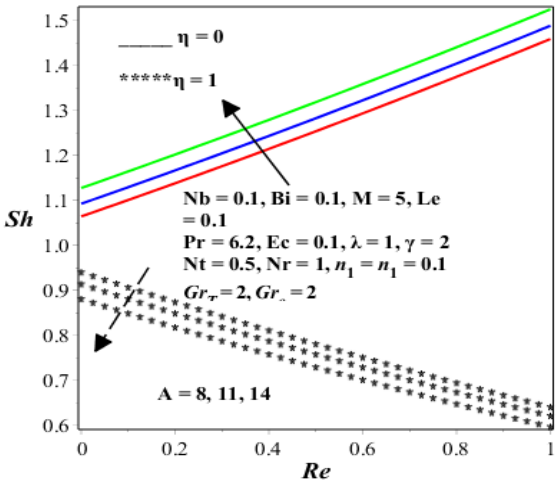

Fig.24: Sherwood number as A versus Re increase

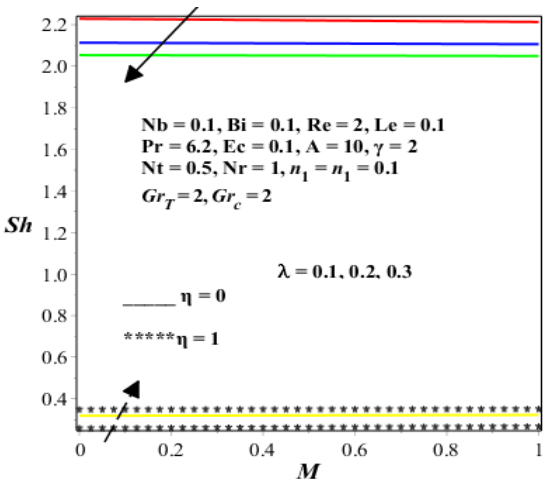

Fig.25: Sherwood number as λ versus M increase

4.5. Entropy Generation Rate

Figures 26-31 illustrate the influence of parameter variations on the entropy generation profile. In figure 26, it is observed that entropy production rate is higher along the channel core region and lower at the walls. An increase in the flow rate via pressure gradient parameter (A) will enhance the entropy generation rate while a rise in suction / injection Reynolds number (Re) at the walls will slow down the entropy production rate in the flow system. Figure 27 shows that entropy production is augmented with combined increase in both thermal and nanoparticles concentration Grashof numbers. This may be attributed to a rise in fluid friction together with heat and mass transfer as these parameters increase. Figure 28 revealed that both magnetic field and couple stress parameter slow down the entropy generation rate. This may be due to a fall in fluid friction irreversibility as these parameters increase. Interestingly, the entropy production is enhanced by a rise in Brownian motion of nanoparticles while a rise in thermophoresis parameter slow down the entropy generation rate as shown in figure 29. As the Lewis number and Biot number increase in figure 30, the entropy generation rate increases at the left wall and decreases at the right wall. This can be attributed to a rise in thermal diffusivity and the convective heat transfer at the left wall leading to a rise in heat transfer irreversibility and entropy generation. In figure 31, it is observed that the both thermal radiation (Nr*)* and temperature difference parameter (γ) enhance entropy production in the flow system.

[DOI: 10.1299/jtst.2017jtst0033]

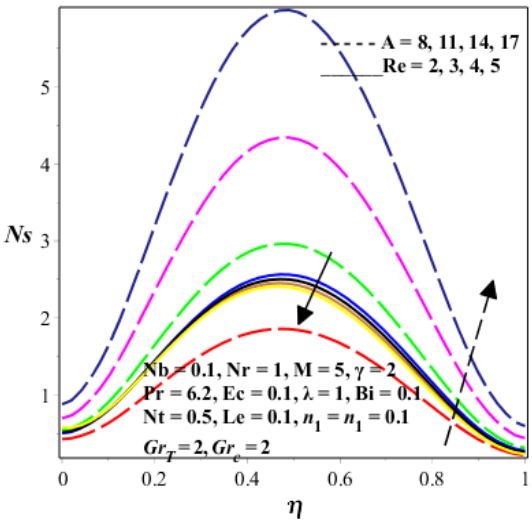

Fig.26: Entropy generation rate as Re and A increase

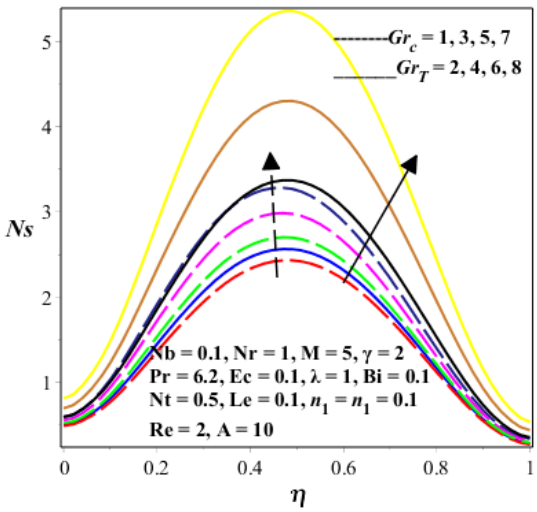

Fig.27: Entropy generation rate as Gr_T and Gr_c increase

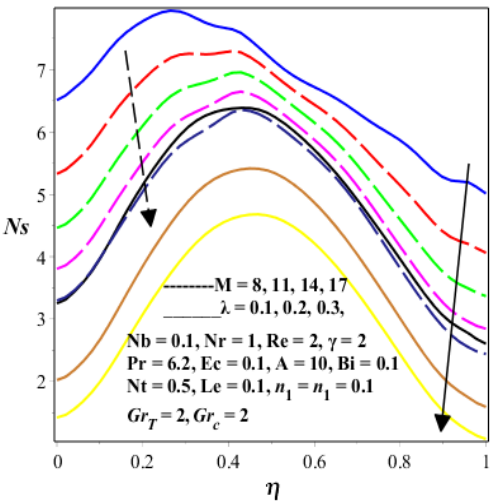

Fig.28: Entropy generation rate as M and λ increase

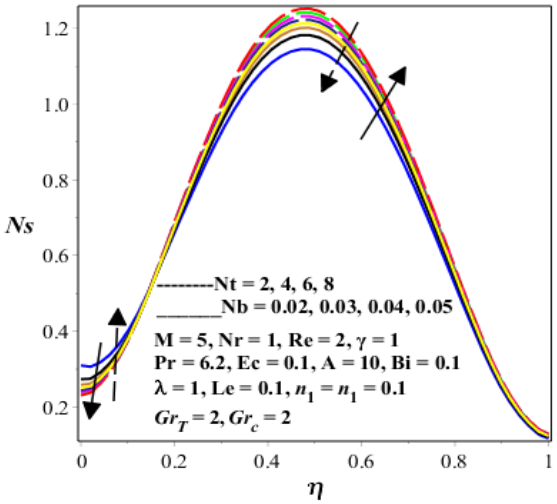

Fig.29: Entropy generation rate as Nt and Nb increase

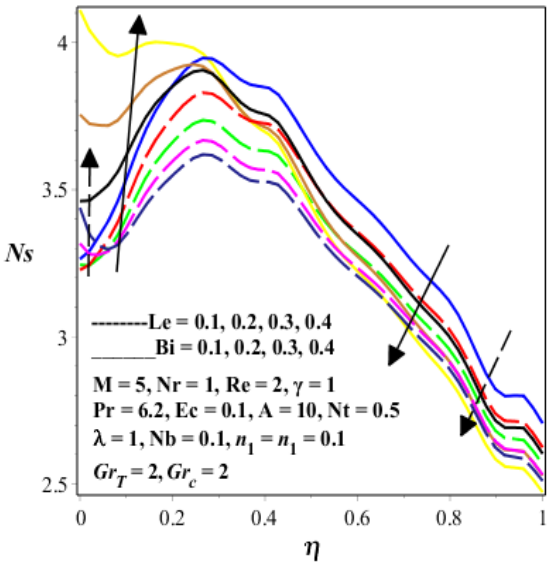

Fig.30: Entropy generation rate as Le and Bi increase

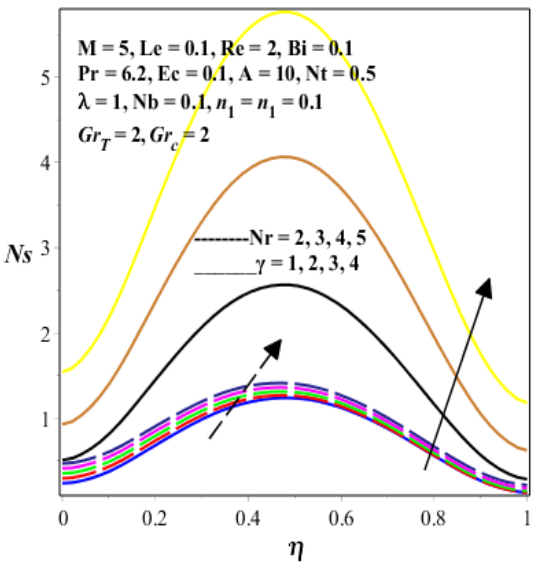

Fig.31: Entropy generation rate as Nr and γ increase

[DOI: 10.1299/jtst.2017jtst0033]

4.6. Bejan Number

Figures 32-37 depict the effects various thermophysical parameters on the Bejan number. It is noteworthy that the Bejan number is higher at the left wall as compare to the right wall. This confirmed the dominant effect of heat transfer irreversibility at the left wall region as expected, since the convective heat transfer to the ambient environment takes place at the left wall. Meanwhile, a rise in the parameter values of Re, A, Gr_T and Gr_c as shown in figures 32-33 decreases the Bejan number, thus enhance the combined effects of fluid friction with nanoparticles mass transfer irreversibility. Both magnetic field and couple stress parameters augment the dominant effects heat transfer irreversibility (see figure 34). The Bejan number at the left wall increases with Brownian motion parameter but and decreases with thermophoresis parameter as depicted in figure 35. In figure 36, we observed that the Bejan number at the left wall is enhanced and reduced at right wall with increasing Biot number. An increase in Lewis number diminishes in the Bejan number. Moreover, it is observed in figure 37 that both thermal radiation and temperature difference parameters enhance the Bejan number, consequently, the dominant effect of heat transfer irreversibility is boosted.

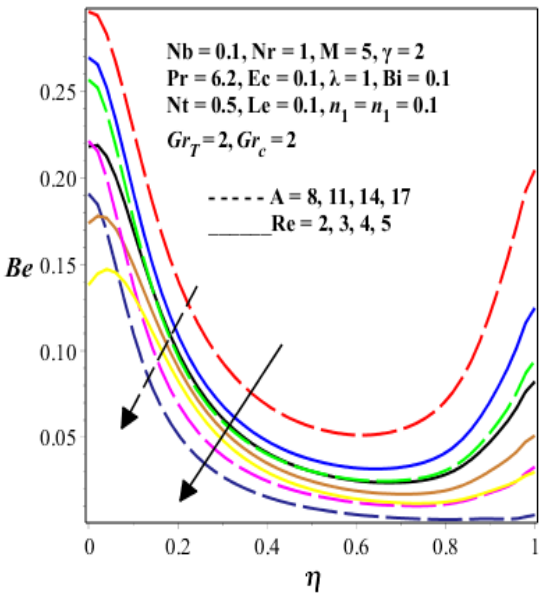

Fig.32: The Bejan number profile as Re and A increase

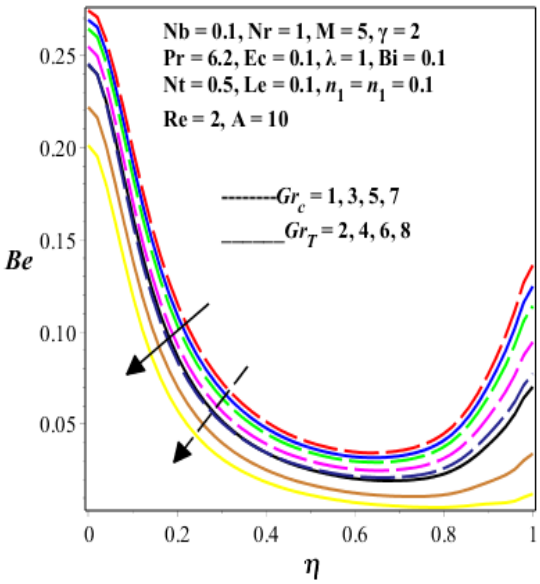

Fig.33: The Bejan number profile as Gr_T and Gr_c increase

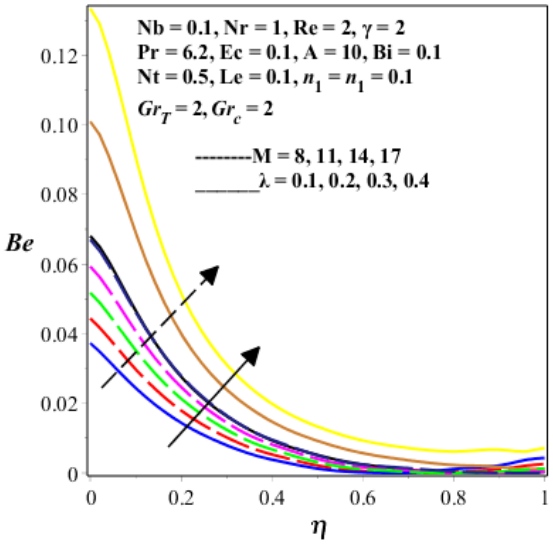

Fig.34: The Bejan number profile as M and λ increase

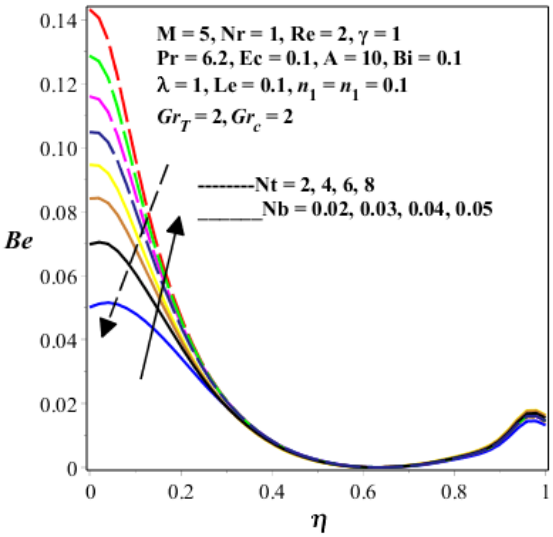

Fig.35: The Bejan number profile as Nt and Nb increase

[DOI: 10.1299/jtst.2017jtst0033]

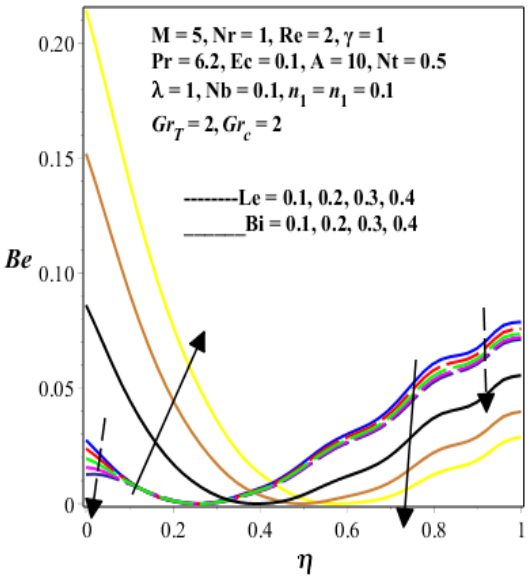

Fig.36: The Bejan number profile as Le and Bi increase

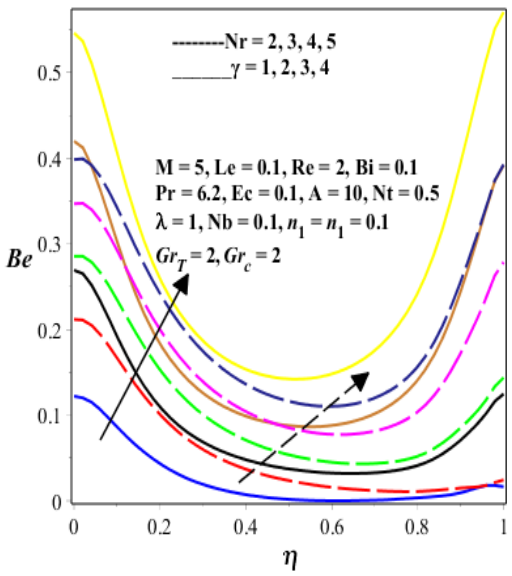

Fig.37: The Bejan number profile as Nr and γ increase

5. Conclusion

The first and second laws (of thermodynamics) aspects of MHD mixed convective flow of radiating couple stress nanofluid through a channel with permeable walls are investigated numerically using shooting technique coupled with a Runge-Kutta-Fehlberg integration scheme. The computational results are presented through figures with respect to the the effects of A, Gr_T, Gr_c, Nb, Nt, M, Nr, Le, λ, γ, Bi on the velocity, temperature, concentration, skin friction, Nusselt number, Sherwood number, entropy generation rate and Bejan number. It is observed that the energy conversion processes in the flow system are accompanied by an irreversible increase in entropy, which leads to a decrease in exergy (available energy). However, the entropy production can be effectively minimized by combining appropriate values of various thermophysical parameters controlling the system for efficient operation. This will invariably result in more efficient designs of various flow and thermal systems including micro scale systems such as micro-mixing technologies and heat exchangers. It is hoped that our findings will serve as a stimulus for further theoretical studies and experimental work which appears to be lacking at present.

References

Abbas, Z., Naveed, M.,Sajid, M.,Hydromagnetic slip flow of nanofluid over a curved stretching surface with heat generation and thermal radiation, Journal of Molecular Liquids, Vol. 215, (2016),756-762.

Adesanya, S. O., Makinde, O. D., Heat transfer to magnetohydrodynamic non-Newtonian couple stress pulsatile flow between two parallel porous plates, Zeitschrift f¨ur Naturforschung, Vol. 67a, (2012), 647 – 656.

Bejan, A., Entropy Generation Minimization, CRC, Boca Raton, NY, 1996.

Buongiorno, J., Convective transport in nanofluids, ASME J. Heat Transfer, Vol.128, (2006), 240-250.

Chiang, H. L., Hsu, C. H., Lin, J. R., Lubrication performance of finite journal bearings considering effects of couple stresses and surface roughness, Tribol. Int., *Vol. 37, (2004), 297-307.*

Cho, C. C., Heat transfer and entropy generation of natural convection in nanofluid-filled square cavity with partially-heated wavy surface, International Journal of Heat & Mass Transfer, Vol.77 (4), (2014), 818-827.

Choi, S., Enhancing thermal conductivity of fluids with nanoparticles, In: Siginer DA, Wang HP (eds.) Developments and applications of non-newtonian flows, FED–231, MD–66, ASME, (1995), 99–105.

Das, S., Banu, A. S., Jana, R. N., Makinde, O. D., Entropy analysis on MHD pseudo-plastic nanofluid flow through a vertical porous channel with convective heating, Alexandria Engineering Journal, Vol. 54(3), (2015), 325-337.

[DOI: 10.1299/jtst.2017jtst0033]

Dulal, P., Rudraiah, L. M., Devanathan, R., A couple stress model of blood flow in the microcirculation, Bull. Math. Biol., Vol. 50, (1988) 329-344.

Eastman, J. A., Choi, S.U.S., Li, S., Yu, W., Thompson, L. J., Anomalously increased effective thermal conductivity of ethylene glycol-based nanofluids containing copper nanoparticles, Appl. Phys. Lett., Vol.78, (2001), 718-720.

Eegunjobi, A. S., Makinde,O. D.,Irreversibility analysis of hydromagnetic flow of couple stress fluid with radiative heat in a channel filled with a porous medium, Results in Physics, Vol. 7, (2017a), 459-469.

Eegunjobi, A. S., Makinde,O. D.,MHD mixed convection slip flow of radiating Casson fluid with entropy generation in a channel filled with porous media, Defect and Diffusion Forum, Vol. 374, (2017b) 47-66.

Leong, K. Y., Saidur, R., Khairulmaini, M., Heat transfer and entropy analysis of three different types of heat exchangers operated with nanofluids, International Communications in Heat & Mass Transfer, Vol. 39(6), (2012), 838-843.

Lin, J. R., Hung, C. R., Combined effects of non-Newtonian couple stresses and fluid inertia on the squeeze film characteristics between a long cylinder and an infinite plate, Fluid Dyn. *Res*., Vol.39(8), (2007), 616–639.

Mahmoudi,A.H., Pop, I., Shahi, M., Talebi, F., MHD natural convection and entropy generation in a trapezoidal enclosure using Cu–water nanofluid, Computers & Fluids Vol.72, (2013), 46–62.

Makinde, O.D., Eegunjobi, A. S.,Entropy analysis of thermally radiating MHD slip flow of Casson fluid in a microchannel filled with saturated porous media, Journal of Porous Media, Vol 19(9), (2016), 799-810.

Makinde, O. D., Khan, W. A., Culham,J. R., MHD variable viscosity reacting flow over a convectively heated plate in a porous medium with thermophoresis and radiative heat transfer, International Journal of Heat and Mass Transfer, Vol.93, (2016a), 595–604.

Makinde, O. D., Iskander, T., Mabood, F., Khan, W. A., Tshehla, M. S., MHD Couette-Poiseuille flow of variable viscosity nanofluids in a rotating permeable channel with Hall effects, Journal of Molecular Liquids, Vol. 221, (2016b), 778-787.

Makinde, O. D.,Animasaun, I. L.,Bioconvection in MHD nanofluid flow with nonlinear thermal radiation and quartic autocatalysis chemical reaction past an upper surface of a paraboloid of revolution, International Journal of Thermal Sciences, Vol. 109, (2016c), 159-171.

Mkwizu, M.H., Makinde, O. D.,Entropy generation in a variable viscosity channel flow of nanofluid with convective cooling, Comptes Rendus Mécanique, Vol. 343, (2015), 38-56.

Na,T. Y., Computational methods in engineering boundary value problem. Academic Press, 1979.

Naduvinamani,N. B., Fathima, S. T., Hiremath, P. S., Hydrodynamic lubrication of rough slider bearings with couple stress fluids, Tribol. Int., Vol.36(12), (2003), 949–959.

Ozisik, M. N., Radiation transfer and interactions with conduction and convection. Wiley-Inter-Science Publication, USA, 1973.

Raptis, A., Radiation and free convection flow through a porous medium, Int. Commun *Heat Mass Transfer,* Vol. 25, (2009),289–295.

Rosseland, S., Theoretical astrophysics. Oxford University, New York, NY, USA, 1936.

Selvakumar, R. D., Dhinakaran, S., Forced convective heat transfer of nanofluids around a circular bluff body with the effects of slip velocity using a multi-phase mixture model, International Journal of Heat and Mass Transfer, Vol.106, (2017), 816–828.

Stokes, V. K., Couple stesses in fluids, Phy. of Fluids, Vol. 9, (1966), 1717-1715.

Wang, X., Xu, X., Choi, S.U.S., Thermal conductivity of nanoparticle fluid mixture, J. Thermophys. *Heat Transfer*, Vol.13, (1999), 474-480.

Woods, L.C., Thermodynamics of Fluid Systems. Oxford University Press, Oxford, UK; 1975.

[DOI: 10.1299/jtst.2017jtst0033]